Validating the Efficiency of the FeS2 Method for Elucidating the Mechanisms of Contaminant Removal Using Fe0/H2O Systems

Authors:

Minhui Xiao, Xuesong Cui, Rui Hu, Willis Gwenzi, Chicgoua Noubactep

Date Submitted: 2021-04-16

Keywords: zero-valent iron, removal mechanism, MB method, FeS2 method, dye discoloration

Abstract:

There is growing interest in using pyrite minerals (FeS2) to enhance the efficiency of metallic iron (Fe0) for water treatment (Fe0/H2O systems). This approach contradicts the thermodynamic predicting suppression of FeS2 oxidation by Fe0 addition. Available results are rooted in time series correlations between aqueous and solid phases based on data collected under various operational conditions. Herein, the methylene blue method (MB method) is used to clarify the controversy. The MB method exploits the differential adsorptive affinity of MB onto sand and sand coated with iron corrosion products to assess the extent of Fe0 corrosion in Fe0/H2O systems. The effects of the addition of various amounts of FeS2 to a Fe0/sand mixture (FeS2 method) on MB discoloration were characterized in parallel quiescent batch experiments for up to 71 d (pH0 = 6.8). Pristine and aged FeS2 specimens were used. Parallel experiments with methyl orange (MO) and reactive red 120 (RR120) enabled a better discussion of the achieved results. The results clearly showed that FeS2 induces a pH shift and delays Fe precipitation and sand coating. Pristine FeS2 induced a pH shift to values lower than 4.5, but no quantitative MB discoloration occurred after 45 d. Aged FeS2 could not significantly shift the pH value (final pH ? 6.4) but improved the MB discoloration. The used systematic sequence of experiments demonstrated that adsorption and coprecipitation are the fundamental mechanisms of contaminant removal in Fe0/H2O systems. This research has clarified the reason why a FeS2 addition enhances the efficiency of Fe0 environmental remediation.

Record Type: Published Article

Submitted To: LAPSE (Living Archive for Process Systems Engineering)

Citation (overall record, always the latest version):	LAPSE:2021.0153
Citation (this specific file, latest version):	LAPSE:2021.0153-1
Citation (this specific file, this version):	LAPSE:2021.0153-1v1

DOI of Published Version: https://doi.org/10.3390/pr8091162

License: Creative Commons Attribution 4.0 International (CC BY 4.0)

processes

MDPI

Article

Validating the Efficiency of the FeS_2 Method for Elucidating the Mechanisms of Contaminant Removal Using Fe^0/H_2O Systems

Minhui Xiao [1], Xuesong Cui [1], Rui Hu [1,*], Willis Gwenzi [2] and Chicgoua Noubactep [3,4,*]

1 School of Earth Science and Engineering, Hohai University, Fo Cheng Xi Road 8, Nanjing 211100, China; xiaominhui@hhu.edu.cn (M.X.); cuixuesong@hhu.edu.cn (X.C.)
2 Biosystems and Environmental Engineering Research Group, Department of Soil Science and Agricultural Engineering, University of Zimbabwe, P.O. Box MP167, Mt. Pleasant, Harare 921, Zimbabwe; wgwenzi@agric.uz.ac.zw
3 Applied Geology, University of Göttingen, Goldschmidtstraße 3, D-37077 Göttingen, Germany
4 Centre for Modern Indian Studies (CeMIS), University of Göttingen, Waldweg 26, D-37073 Göttingen, Germany
* Correspondence: rhu@hhu.edu.cn (R.H.); cnoubac@gwdg.de (C.N.)

Received: 5 August 2020; Accepted: 11 September 2020; Published: 16 September 2020

Abstract: There is growing interest in using pyrite minerals (FeS_2) to enhance the efficiency of metallic iron (Fe^0) for water treatment (Fe^0/H_2O systems). This approach contradicts the thermodynamic predicting suppression of FeS_2 oxidation by Fe^0 addition. Available results are rooted in time series correlations between aqueous and solid phases based on data collected under various operational conditions. Herein, the methylene blue method (MB method) is used to clarify the controversy. The MB method exploits the differential adsorptive affinity of MB onto sand and sand coated with iron corrosion products to assess the extent of Fe^0 corrosion in Fe^0/H_2O systems. The effects of the addition of various amounts of FeS_2 to a Fe^0/sand mixture (FeS_2 method) on MB discoloration were characterized in parallel quiescent batch experiments for up to 71 d ($pH_0 = 6.8$). Pristine and aged FeS_2 specimens were used. Parallel experiments with methyl orange (MO) and reactive red 120 (RR120) enabled a better discussion of the achieved results. The results clearly showed that FeS_2 induces a pH shift and delays Fe precipitation and sand coating. Pristine FeS_2 induced a pH shift to values lower than 4.5, but no quantitative MB discoloration occurred after 45 d. Aged FeS_2 could not significantly shift the pH value (final pH ≥ 6.4) but improved the MB discoloration. The used systematic sequence of experiments demonstrated that adsorption and coprecipitation are the fundamental mechanisms of contaminant removal in Fe^0/H_2O systems. This research has clarified the reason why a FeS_2 addition enhances the efficiency of Fe^0 environmental remediation.

Keywords: dye discoloration; FeS_2 method; MB method; removal mechanism; zero-valent iron

1. Introduction

Metallic iron (Fe^0), commonly termed as zero-valent iron (ZVI), is widely used for decentralized safe drinking water provision [1–3] and environmental remediation [4–6]. Its suitability to remove a large array of biological and chemical pollutants from aqueous solutions has been demonstrated over the past three decades [7–14]. However, Fe^0 is mostly considered as a reducing agent ($E^0 = -0.44$ V for the redox couple Fe^{II}/Fe^0) for reducible species [4,12,15]. This reductionist but wrong view has been motivated by the failure to consider the inherent features of aqueous iron corrosion, which results in the shortcomings of the Fe^0 remediation technology [9]. These features include: (i) the increase of the pH value, coupled with subsequent shielding of the Fe^0 surface by an oxide scale (reactivity loss),

and (ii) the volumetric expansive nature of iron corrosion, coupled with a decrease of the hydraulic conductivity (permeability loss). A profound understanding of the interactions of pollutants within Fe^0/H_2O systems resulting in their removal from the aqueous phase is needed for designing of the next generation of sustainable Fe^0 remediation systems.

Information regarding the mechanisms of contaminant removal in Fe^0/H_2O systems is confusing. For example, Matheson and Tratnyek [16] reported that carbon tetrachloride (CCl_4) is reductively transformed by electrons from the metal body (direct reduction). Jiao et al. [17] systematically investigated the $Fe^0/CCl_4/H_2O$ system and concluded that direct reduction (electron from Fe^0) did not play any significant role in the observed CCl_4 reductive transformation. Instead, Jiao et al. [17] concluded that CCl_4 was chemically reduced by primary iron corrosion products (Fe^{II} and H/H_2 species) (indirect reduction). The results of Jiao et al. [17] validate the concept that contaminants are removed predominantly by adsorption and coprecipitation, while chemical reduction might occur to a lesser extent [18–22]. According to Xiao et al. [14], the concept that adsorption and coprecipitation are the fundamental mechanisms of contaminant removal in Fe^0/H_2O systems has been widely ignored by active researchers during the past decade. Given that related articles ignoring this concept were published in readily accessible journals, there is still a need for more convincing experimental evidence.

A myriad of approaches aiming at improving the efficiency of Fe^0/H_2O remediation systems have been presented. Relevant approaches include alloying with more noble metals (e.g., Pd and Pt), using nanoscale Fe^0, and using weak magnetic fields [4,23,24]. However, they are equally not well-rationalized [25]. For example, on the one hand, nanoscale Fe^0 particles are passivated in the same way as microscale ones [26]. On the other hand, hybrid systems have been introduced as a tool to sustain the efficiency of Fe^0/H_2O systems [23,24]. The tested systems include: (i) $Fe^0/Fe_3O_4/Fe^{2+}$ [27,28], (ii) Fe^0/FeS_2 [15,29], (iii) Fe^0/MnO_2 [30,31], and (iv) Fe^0/sand [32–34]. However, the majority of available reports stemmed from the misconception that Fe^0 is an environmental reducing agent [14,25,35]. The comparability of the achieved results is further complicated by the fact that the experimental operational conditions varied widely among the studies [14,36]. The relevant operational parameters include the nature of contaminants and agitation rates. Given the large number of species likely to be contaminants on a site-specific basis, the need to work with selected probe species has been highlighted [37–39]. In this regard, methylene blue (MB) has been demonstrated as an indicator of the reactivity of Fe^0/H_2O remediation systems (MB method) [40,41]. The MB method is based on the differential affinity of MB for sand and sand coated with iron corrosion products (FeCPs), as demonstrated in the historical work of Mitchell et al. [42].

The suitability of the MB method for the characterization of the dynamic process of iron corrosion arises from the evidence that, in a Fe^0/sand/H_2O system, sand is progressively coated by in-situ generated FeCPs [40,41]. The negatively charged sand is initially an excellent adsorbent for positively charged MB (a cation). As sand progressively adsorbs in-situ generated Fe^{2+} and Fe^{3+} (two cations), its surface is covered by an oxide layer, which is positively charged. Thus, coated sand is repulsive for cationic MB. In other words, rationally selecting the relative amounts of Fe^0 and sand, the initial MB concentration, and the experimental duration enables a realistic evaluation of the extent of FeCPs generation without any Fe mass balance nor instrumental analysis (e.g., scanning electron microscopy-SEM). For this reason, MB is an operational reactive tracer and not a model micropollutant [40].

Another key feature of the Fe^0/H_2O system is the pivotal role of in-situ generated FeCPs, which are critical for its efficiency and sustainability. In particular, controlling their availability is a powerful tool to understand their role in the dynamic process of contaminant removal [43–45]. From the presented approaches, the method involving shifting the pH values by adding a reactive pyrite (FeS_2) mineral to lower values, while monitoring the efficiency of the Fe^0/H_2O system as the pH subsequently increased, is used herein (FeS_2 method). Regarding FeS_2 as a pH-shifting agent seemingly overlooks the evidence that galvanic interactions exist in the $Fe^0/FeS_2/H_2O$ system. Galvanic interactions are a well-known phenomenon both in corrosion science (Fe^0) [15,46] and mineral processing (FeS_2) [47–50]. In particular,

rooting the reasoning on galvanic interactions, reference [49] suggested using Fe^0 (E^0 = −0.44 V) to galvanically prevent FeS_2 (E^0 = 0.25 V) oxidation [49]. In this process, Fe^0 is anodically oxidized, and Fe^{2+} ions are transported to cathodic sites on the FeS_2 surface, where a protective Fe-oxyhydroxide layer develops. Clearly, Seng et al. [49] demonstrated the suitability of a Fe^0 addition to suppress FeS_2 oxidation. This is exactly the opposite goal of using Fe^0/FeS_2 systems in water remediation [15]. This controversy calls for a more detailed investigation of the dynamics within the $Fe^0/FeS_2/H_2O$ system.

The suitability of the FeS_2 method for the characterization of the dynamic process of contaminant removal in Fe^0/H_2O systems arises from the fact that shifting the pH to lower values increases the solubility of iron [15]. If the pH is decreased to values lower than 4.5, iron precipitation will occur in the bulk solution and not in the vicinity of Fe^0. In other words, the FeS_2 addition certainly decreases the pH of the system. However, the impact of the pH shift on the decontamination process depends on the extent of the pH shift (minimum pH achieved) and the final pH value. Both the minimum pH and the final pH values depend on several operational factors, including the relative amounts of Fe^0 and FeS_2 and the experimental duration. It is recalled that Fe^0 corrosion increases the pH value while FeS_2 oxidation reduces it [15]. The FeS_2 method implies that the FeS_2 reactivity might be exhausted during the experiment, so that, for longer experimental durations, the final pH should be equal or higher than the initial value.

In the present work, the MB method [41] and the FeS_2 method [44] were combined in order to better characterize the dynamic process of iron corrosion and the interactions within Fe^0/H_2O systems, accounting for contaminant removal. Parallel MB discoloration batch experiments in Fe^0/sand, FeS_2/sand, and Fe^0/FeS_2/sand systems were undertaken for up to 71 d. Under these conditions, various amounts of FeCPs were generated for differential MB discoloration. The FeS_2 mineral was used in its pristine form (pristine FeS_2) and after aging for six months (aged FeS_2). Additional experiments were performed for the discoloration of methyl orange (MO) and reactive red 120 (RR120); the results are compared.

2. Materials and Methods

2.1. Solutions

2.1.1. Dyes

Methylene blue (MB) was used as a tracer of reactivity [41], while methyl orange (MO) and reactive red 120 (RR120) were used as model organic micropollutants [15,51]. The three dyes are widely used to characterize the suitability of various systems for water treatment [51–54]. The used dyes were of analytical grade. MB was supplied by Sinopharm Chemical Reagent Co., Ltd. (Shanghai, China), MO by Tianjin Chemical Reagent Research Institution Co., Ltd. (Tianjin, China), and RR120 by Sigma-Aldrich® (St. Louis, MO, USA). The dyes were selected due to: (i) similarity in their molecular size (MB and MO) and (ii) differences in their affinity to positively charged iron oxides (Table 1) [45,55]. RR120 was included, because it has a higher molecular size relative to MO. The initial dye concentration used was 10 mg L^{-1}, equivalent to 31.5 μM for MB, 30.7 μM for MO, and 6.8 μM for RR120. The dye working solutions were prepared by dissolving the corresponding crystals in deionized water. The pH values of the initial solution were 6.5 (MB), 6.6 (MO), and 7.0 (RR120).

Table 1. Some physicochemical characteristics of three tested dyes. MW stands for molecular weight. Adapted from Gatcha-Bandjun et al. [45].

Dye	Symbol	Formula	MW (g mol^{-1})	Nature	λ_{max} (nm)
Methylene blue	MB	$C_{16}H_{18}ClN_3S{\cdot}3H_2O$	319.00	cationic	664.5
Methyl orange	MO	$C_{14}H_{12}N_3O_3NaS$	327.34	anionic	464.0
Reactive red 120	RR120	$C_{44}H_{30}Cl_2N_{14}O_{20}S_6$	1469.98	anionic	515.0

Other chemicals used in this study included L(+)-ascorbic acid and L-ascorbic acid sodium salt. Ascorbic acid also degrades dyes (in particular, MO) and eliminates interference during iron determination [30,45].

2.1.2. Iron

A standard iron solution (Testing & Certification Co., Ltd., Beijing, China) (1000 mg L^{-1}) from the General Research Institute for Nonferrous Metals was used to calibrate the UV/VIS spectrophotometer (Shanghai Jinghua Technology Instrument Co., Ltd, Shanghai, China) used for analysis. All other chemicals used were of analytical grade. In preparation for the spectrophotometric analysis, ascorbic acid was used to reduce Fe^{III} in the solution to Fe^{II}. 1,10 orthophenanthroline was used as reagent for Fe^{II} complexation.

2.2. Solid Materials

2.2.1. Metallic Iron (Fe^0)

The used Fe^0 material was purchased from the Shanghai Institute of Fine Technology (Shanghai, China). The Fe^0 used in the current study has been used and described in earlier studies by our research group [45,56]. The material is available as scrap iron with a particle size between 0.05 and 5 mm. Its elemental composition, as specified by the supplier, was: Fe: >99.99%, C: <0.1%, N: <0.1%, and O: <0.1%. Its k_{Phen} value was 13 mg h^{-1} [56]. The k_{Phen} value is the kinetic parameter of Fe^0 dissolution in a 2-mM 1,10 orthophenanthroline solution, which characterizes the material's intrinsic reactivity [57]. The material was used without any further pretreatment. Fe^0 has been previously proven to be a powerful discoloration agent for MB specifically because the discoloration agents are progressively generated in situ [58,59]. Therefore, the discoloration capacity of used Fe^0 cannot be exhausted within the experimental duration (up to 71 d).

2.2.2. Sand

The used sand was China ISO standard sand, which was used as received without any further pretreatment or characterization. The particle size was between 1.25 and 2.00 mm. Sand was used because of its worldwide availability and its use as an admixing agent to prevent a rapid permeability loss in Fe^0/H_2O systems [60,61].

2.2.3. Pyrite (FeS_2)

The used FeS_2 mineral was from Tongling City, Anhui Province, China. The particle size was between 38 and 48 µm. Its weight composition was 46.0% Fe and 52.2% S; this is equivalent to a purity of 98.2% [29]. FeS_2 was used because of its demonstrated suitability as a pH-shifting agent in Fe^0/H_2O systems [62–65].

2.3. Dye Discoloration

Quiescent batch experiments with pristine FeS_2 were conducted in glass test tubes for an experimental duration of 41 d. Dye discoloration was initiated by adding 20.0 mL of the dye solution to a test tube containing 0.0 or 0.1 g of Fe^0, 0.0 to 0.6 g of FeS_2, and 0.0 or 0.5 g of sand. Thus, Fe^0/FeS_2/sand mixtures contain the same mass of Fe^0 (0.1 g), the same mass of sand (0.5 g), and varying FeS_2 loadings (0.05 to 0.60 g). The corresponding mass loadings of the individual materials varied from 0.0 to 30.0 g L^{-1}. The blank corresponds to no material addition (0.0 g of Fe^0, FeS_2, and sand). Three single aggregate (Fe^0, FeS_2, and sand) and two binary (Fe^0/FeS_2 and Fe^0/sand) systems were investigated. The discussion is mainly focused on the ternary systems. The seven Fe^0/FeS_2/sand systems contained 0.05, 0.1, 0.2, 0.3, 0.4, 0.5, and 0.6 g of FeS_2 (2.5 to 30.0 g L^{-1}) respectively. Besides sustaining the MB method, the sand addition was intended to avoid compaction of the material by gelatinous FeCPs (cementation) [61].

Three sets of experiments were conducted. The first set of experiments using pristine FeS_2 were initiated in April 2019, lasting for 41 d. In October 2019, a second set of experiments using the aged form of the same FeS_2 mineral (aged FeS_2) were initiated while extending the dyes to RR120. The second set of experiments lasted for 45 d. The third and last set of experiments entailed following the time-dependent changes in the ternary system for up to 71 d using the following material mixture: Fe^0 (0.1 g or 5.0 g L^{-1}) + FeS_2 (0.1 g or 5.0 g L^{-1}) + sand (0.5 g or 25.0 g L^{-1}). In addition, parallel experiments with each dye were performed.

The efficiency of individual systems for dye discoloration was characterized at laboratory temperatures (about 25 ± 2 °C). The final pH values, the iron concentrations, and the residual dye concentrations were recorded (t = 41 d for pristine FeS_2 and t = 45 d for aged FeS_2). All experiments were carried out in triplicates under laboratory (oxic) conditions. The test tubes were protected from direct sunlight, as described in earlier studies [30,45,56].

2.4. Analytical Methods

Aqueous dye and iron concentrations were determined by a 752 UV/VIS Spectrophotometer (automatic) (Shanghai Jing Hua Technology Instrument Co., LTD, Shanghai, China). The respective working wavelengths for MB, MO, RR120, and iron were 664.5, 464.0, 515.0, and 510.0 nm (Table 1). Cuvettes with a 1.0-cm light path were used. The iron determination followed the 1,10 orthophenanthroline method [66]. The spectrophotometer was calibrated for dye concentrations ≤15.0 mg L^{-1} and iron concentrations ≤10.0 mg L^{-1}. The pH values were measured by combined glass electrodes (INESA Scientific Instrument Co., Shanghai, China).

2.5. Presentation of Experimental Results

In order to characterize the magnitude of the tested systems for dye discoloration, the discoloration efficiency (E) was calculated (Equation (1)):

$$E = [1 - (C/C_0)] \times 100\% \quad (1)$$

where C_0 was the initial aqueous dye concentration (10.0 mg L^{-1}), while C gave the final residual dye concentration. The operational initial concentration (C_0) for each case was acquired from a triplicate control experiment without additive materials (so-called blank). This procedure was mainly to account for experimental errors due to dye adsorption onto the walls of the test tubes.

3. Results and Discussion

Experiments with pristine FeS_2 are considered the reference system for the discussion. April 2019 is operationally considered as t_0 = 0, although the same material was already used in previous works [29,35]. The presentation is mostly focused on the difference between pristine and aged FeS_2.

3.1. Evidence for the pH-Shifting Nature of FeS_2

Figure 1 compares the extent of pH shift and the final iron (total iron) concentrations in the Fe^0/FeS_2/sand systems for MB discoloration after 41 d for pristine FeS_2 and 45 d for aged FeS_2. The results for MO discoloration showed a similar trend, with a slightly higher iron concentration for aged FeS_2 (up to 6.0 mg L^{-1}). For pristine FeS_2, the pH value decreased substantially from 7.0 to 4.5 (Figure 1a), while the pH shift was minor (i.e., 0.2 pH units) for aged FeS_2 (Figure 1b). During these long contact times (41 and 45 d), pyrite oxidation by dissolved O_2 should occur quantitatively. The fact that aged FeS_2 was not dissolved suggests that, during the six months of storage time under the laboratory conditions, FeS_2 quantitatively reacted with air oxygen. This statement is supported by the extent of iron dissolution (Figure 1b) and visual observations showing rust stains. While the iron concentration increased from 0.2 to 99 mg L^{-1} as the pristine FeS_2 loading changed from 0 to 24 g L^{-1}, even higher aged FeS_2 loadings (30 g L^{-1}-results not shown) could not induce iron dissolution to

concentrations larger than 0.2 mg L^{-1}. The next sections discuss how iron dissolution and contaminant removal are coupled to each other.

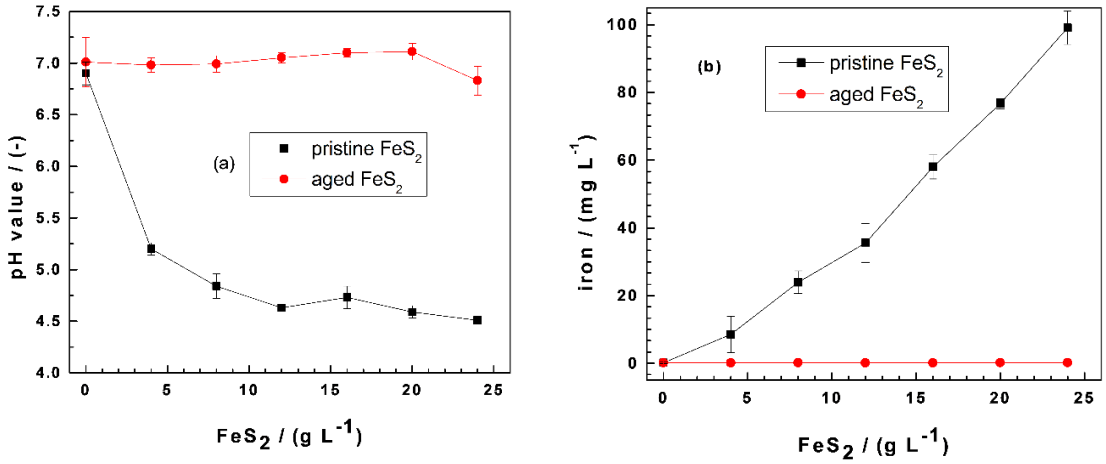

Figure 1. Changes of the (**a**) final pH values and (**b**) iron concentrations as a function of the pyrite (FeS_2) mass loading in Fe^0/FeS_2/sand systems. Experimental conditions: (Fe^0) = 5.0 g L^{-1}, (sand) = 25.0 g L^{-1}, and (MB) = 10.0 mg L^{-1}; t = 41 d for pristine FeS_2, t = 45 d for aged FeS_2, and $V_{solution}$ = 20.0 mL. The lines are not fitting functions; rather, they simply connect points to facilitate visualization. Fe^0: metallic iron and MB: methylene blue.

3.2. MB and MO Discoloration in Fe^0/FeS_2/Sand Systems

Figure 2 compares the effectiveness of Fe^0/FeS_2/sand systems at discoloring MB (Figure 2a) and MO (Figure 2b) as the FeS_2 loading varies from 0 to 25 g L^{-1}. In both cases, the dye discoloration is maximal in the Fe^0/sand system ((FeS_2) = 0 g L^{-1}). This observation is seemingly in contradiction with the evidence that FeS_2 improves the efficiency of Fe^0/H_2O systems for contaminant removal [29,62,67]. However, two key features have to be considered: (i) the presence of sand and (ii) the fact that the systems are quiescent, hence no accelerated mass transfer [19,68]. In other words, the progress of the discoloration process is intentionally slowed down in order to better characterize the interactions accounting for contaminant removal in Fe^0/H_2O systems [43,44,69]. Another seemingly controversial observation is the fact that the pristine FeS_2 system is the most efficient for both MB and MO.

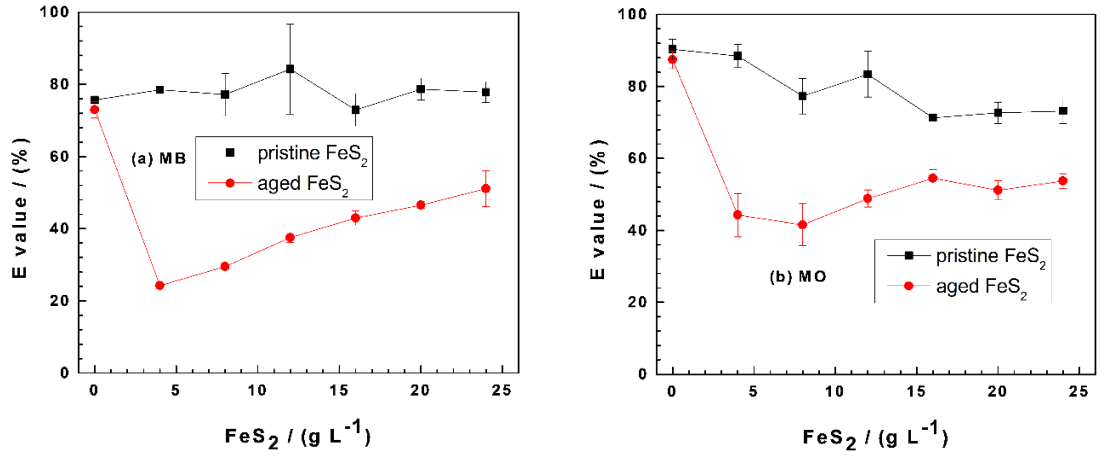

Figure 2. Changes of the percent removal efficiency (E values) for methylene blue (MB) (**a**) and methyl orange (MO) (**b**) as a function of the pyrite (FeS_2) mass loading in Fe^0/FeS_2/sand systems. Experimental conditions: (Fe^0) = 5.0 g L^{-1}, (sand) = 25.0 g L^{-1}, and (dye) = 10.0 mg L^{-1}; t = 41 d for methylene blue (MB), t = 45 d for methyl orange (MO), and $V_{solution}$ = 20.0 mL. The lines are not fitting functions; rather, they simply connect points to facilitate visualization.

Figure 2a shows that the E value for MB removal is almost constant at 80% as the pristine FeS_2 loadings vary from 0 to 25 g L^{-1}. The initial E value (75%) for the aged FeS_2 system first decreases to about 25% at (FeS_2) = 5 g L^{-1} and then progressively increased to 50% at (FeS_2) = 25 g L^{-1}. This observation suggests that, in the presence of pristine FeS_2, MB discoloration is achieved by sand and that its surface was not coated to the extent that MB discoloration is affected. Remember that the surface of sand is negatively charged and is an excellent adsorbent for positively charged MB (a cationic dye) [42]. Once the surface of sand is in-situ covered with positively charge FeCPs, it ceases to adsorb MB. This differential adsorptive behavior of MB on sand and iron-coated sand is the cornerstone of the MB method for investigating the reactivity of the Fe^0/H_2O system [37,40,41]. Clearly, the pristine FeS_2 had no significant impact on MB adsorptive discoloration under the operational conditions. This demonstrates that iron precipitation was not quantitative to the extent that MB coprecipitation was significant. The situation is different in the presence of aged FeS_2 (Figure 2a). There was practically no pH shift (Figure 1a) and no significant increase of the iron concentration (Figure 1b), meaning that the in-situ precipitation of FeCPs in the vicinity of Fe^0 significantly impaired the adsorptive MB discoloration by sand. The observed increase of the E value from 25% to 51% (Figure 2a) is attributed to MB coprecipitation with FeCPs. Such a coprecipitation could not occur in the presence of pristine FeS_2, where MB adsorption on sand was the sole process responsible for discoloration.

Figure 2b shows E ≥ 40%, attesting that MO has a higher affinity to in-situ generated FeCPs. The system with pristine FeS_2 achieved much higher MO discoloration than the aged one, indicating that there were FeCPs formations but no coating of the sand surface. This is the reason why MB adsorption by sand was not disturbed in parallel experiments (Figure 2a). The initial E value of 80% ((FeS_2) = 0 g L^{-1}) decreased to 70% for (FeS_2) = 15 g L^{-1} and remained constant for higher FeS_2 loadings. These results clearly show that FeCPs precipitation was not quantitative and was even less pronounced in systems with low pH values. The lower the pH value, the less the precipitation of FeCPs from the aqueous solution. It is essential to differentiate precipitation in the aqueous phase from precipitation in the vicinity of Fe^0. The behavior of the aged FeS_2 is related to the second case. Here, precipitation is retarded by sand, which has negative charged surfaces that attract ferrous (Fe^{2+}) and ferric (Fe^{3+}) ions, thereby delaying the availability of free FeCPs for dye coprecipitation. This statement is supported by the increasing trend of MO discoloration as the (FeS_2) value increased from 5 to 25 g L^{-1} (Figure 2b).

Section 3.2 has clearly demonstrated the pivotal role of in-situ FeCPs in the process of contaminant removal in Fe^0/H_2O systems. To improve the understanding of the named processes, the results of parallel experiments with the two dyes (MB and MO) and RR120 are presented in the next section.

3.3. RR120 Discoloration Compared to MB and MO in Fe^0/FeS_2/Sand Systems

3.3.1. Changes of pH Value and Iron Concentration

Figure 3a summarizes the results of changes of the pH values as a function of the experimental duration (using aged FeS_2). It is seen that the initial pH value of 7.0 decreased after the addition of FeS_2 to values of 6.8 for RR120 and 6.5 for both MB and MO. There was a further pH decrease until day 5, reaching pH 6.4 for both MB and MO. The very close behavior of the MB and MO systems with respect to changes of the pH values was already reported by Gatcha-Bandjun et al. [45]. After day 5, there is a progressive increase of the pH value with the increasing time. This trend is justified by iron corrosion determining the pH value [14]. Note that, in a $Fe^0/FeS_2/H_2O$ system under oxic conditions, the pH value is determined by two concurrent processes: (i) FeS_2 oxidation lowering the pH and (ii) iron corrosion increasing the pH. These two situations are evident in Figure 3b, where FeS_2 oxidation fixed the pH for (FeS_2) ≤ 5 g L^{-1}, while iron corrosion determined the pH for higher FeS_2 loadings. These results were achieved with aged FeS_2, and the final pH values varied between 6.4 and 7.6 for all investigated systems (variations of only 1.2 pH units). With pristine FeS_2, the window of pH variation would have been larger and the experimental duration longer for similar observations [14]. Noubactep et al. [43] needed up to 120 d to document this trend in their experiments for U(VI) removal.

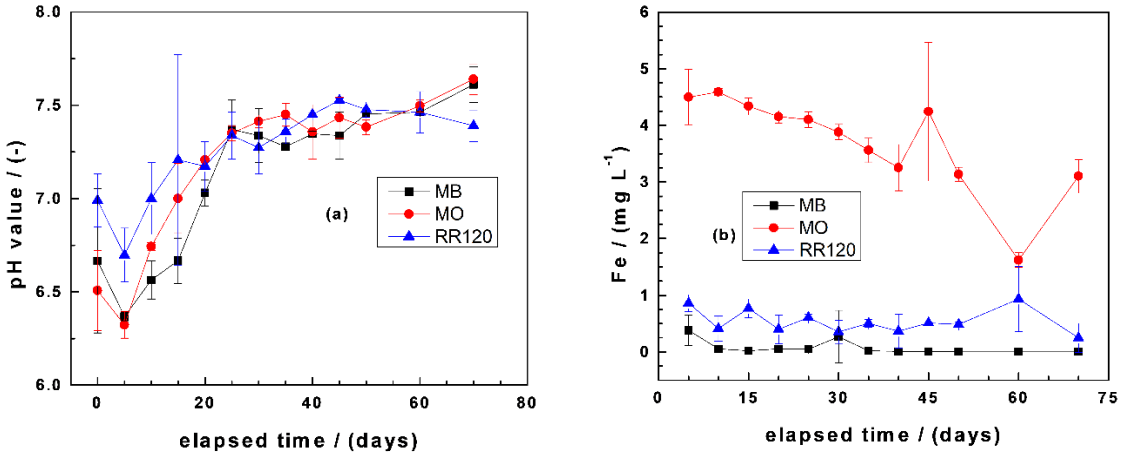

Figure 3. Changes of the final pH values (**a**) and iron concentrations (**b**) as a function of equilibration time in Fe^0/FeS_2/sand systems. Experimental conditions: (Fe^0) = 5.0 g L^{-1}, (FeS_2) = 5.0 g L^{-1}, (sand) = 25.0 g L^{-1}, (dye) = 10.0 mg L^{-1}, and $V_{solution}$ = 20.0 mL. The lines are not fitting functions; rather, they simply connect points to facilitate visualization. MO: methyl orange and RR120: reactive red 120.

Figure 3b summarizes the results of changes of the iron concentrations as a function of the experimental duration. It is seen that more than 3.0 mg L^{-1} Fe is present in the system with MO, while the two other systems exhibited values lower than 1.0 mg L^{-1}. Similar results were reported by Phukan et al. [70] for Orange II and Gatcha-Bandjun et al. [45] for MO and were explained by the formation of relative stable complexes between Fe and MO (and Orange II). The fact that more iron was dissolved in the RR120 system than in the MB system can be justified by steric effects by which a larger RR120 disturbs the formation of an oxide scale on Fe^0, as highlighted by Phukan [71].

The remaining sections will discuss the role of FeCPs on the process of contaminant removal while particularly addressing the role of FeS_2 in sustaining the efficiency of Fe^0/H_2O systems. The time-dependent changes of E values for the three used dyes will be comparatively discussed.

3.3.2. Dye Discoloration

Figure 4 summarizes the results of changes of the E values as a function of the experimental duration for MB, MO, and RR120. It is seen that there is a general trend of increasing E values with increasing equilibration times. However, some species-dependent observations should be highlighted: (i) E values for RR120 continuously increased from the start of the experiment towards the end from 49% to 85%, (ii) E values for MB also increased from 0 to 60 d and then slightly decreased, and (iii) the initial E value of 15% for MO first increased to 45% and, subsequently, increased towards the end (73%). The differences between MB and MO are explained by the differential affinity of both dyes to FeCPs and sand (Section 3.2). For example, in the initial phase (up to 40 d), the higher values for the MB system are attributed to the availability of the sand surface to adsorb MB, because not enough in-situ generated FeCPs have coated the sand. After day 40, the available sand can be considered completely covered with FeCPs, hence the higher E values for MO and, also, the decrease of the E value for MB at the end of the experiments. The higher E values for RR120 than the other two dyes are justified by steric effects due to the larger molecular size of RR120 (Table 1) and, probably, its lower solubility in water [55].

The results in Figure 4 demonstrated the ion-selective nature of the Fe^0/H_2O system. In fact, the competitive nature of dye discoloration by sand and iron-coated sand is demonstrated. This result validates the MB method for the characterization of the Fe^0/H_2O system, while demonstrating the selectivity of the Fe^0/H_2O system for negatively charged species, including bacteria and viruses [72]. In fact, several studies have shown that Fe^0/H_2O systems have the capacity to remove both bacteria and viruses in aqueous systems [1,5,9,62]. Given that pathogens are the most widespread contaminant

worldwide, Fe^0 filters for household drinking water treatments are a good candidate to achieve Goal 6 of the UN Sustainable Development Goals [73,74]

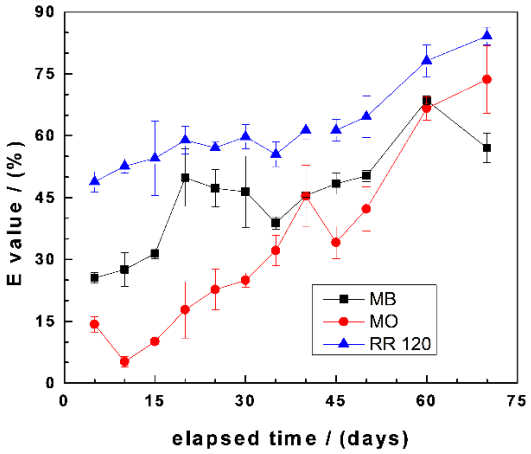

Figure 4. Changes of the dye discoloration efficiency (E) as a function of equilibration time in Fe^0/FeS_2/sand systems. Experimental conditions: $(Fe^0) = 5.0\ g\ L^{-1}$, $(FeS_2) = 5.0\ g\ L^{-1}$, (sand) = 25.0 g L^{-1}, (dye) = 10.0 mg L^{-1}, and $V_{solution}$ = 20.0 mL. The lines are not fitting functions; rather, they simply connect points to facilitate visualization.

3.4. Implications on Contaminant Removal Mechanisms

The idea that Fe^0 is an environmental reducing agent prevails in the recent scientific literature [4,6,36,75]. Admixing Fe^0 with reactive FeS_2 is accordingly regarded as a tool to enhance the reductive capacity of Fe^0 by two mechanisms: (i) freeing the Fe^0 from in-situ generated FeCPs and delay or even avoid "reactivity loss" and (ii) mediating electron transfer to the contaminants by virtue of the semiconductive nature of FeS_2 minerals [15,29,62,76]. This view contradicts the concept of Khudenko [77], demonstrating that Fe^0 can be used to induce the indirect reduction of organic species in water and that copper salts can be used to sustain such indirect reactions. The view of Khudenko [77] was independently introduced by Lipczynska-Kochany et al. [62] using FeS_2 to sustain Fe^0 oxidative dissolution and better discussed the observed reductive degradation of CCl_4 in the presence of Fe^0.

Noubactep et al. [43] presented their results on U(VI) removal in Fe^0/H_2O systems in the peer-reviewed literature in 2003. These results were available in the grey literature two years earlier [78,79]. These authors demonstrated through a sequence of experiments that no significant U(VI) removal is achieved before quantitative iron precipitation occurs. The same authors then proposed the FeS_2 method for the investigation of the mechanism of contaminant removal in Fe^0/H_2O systems [44]. The FeS_2 method entails inducing a pH shift to lower values (ideally, lower than 4.5) by pyrite oxidation and monitoring the contaminant removal when the pH subsequently increased as iron corrosion continues. The results demonstrated that electrochemical reduction (electrons from Fe^0) plays no significant role in the process of U(VI) removal in the presence of Fe^0. This observation implies that contaminant removal is a property of corroding iron: the spontaneous precipitation of iron hydroxides. This corresponds to flocculation, which is a conventional chemical process used in water treatments [80]. Thus, immersed Fe^0 in situ generates contaminant scavengers. Moreover, iron hydroxide precipitation occurs in the presence of trace amounts of contaminants, which are simply occluded via coprecipitation [14,18,19,81,82]. Iron hydroxide precipitation on FeS_2 corresponds to the mechanism of acidification suppression, as recently suggested by Seng et al. [49], and is thus in tune with the thermodynamics of the system.

Surprisingly, all results published after 2006 and claiming that FeS_2 sustains electrochemical contaminant reductions in Fe^0/H_2O systems have not considered the FeS_2 method and the three related references published in Environmental Science & Technology (2003) [43], Environmental Chemistry (2005) [44], and the Journal of Hazardous Materials (2006) [83]. These three journals are from three

different publishers (ACS, CSIRO, and Elsevier, respectively) and can be regarded as authoritative. The rationale for this oversight could be the plethora of scientific articles on the broad topic of "remediation using Fe^0". However, it is the responsibility of individual researchers and research groups to make sure that our common database reflects the state-of-the-art knowledge. The present work was designed to address this issue while highlighting to all stakeholders, including editorial boards of scientific journals, that "recent is not whole". Specifically, there is a trend to recommend recent references, and the technical management of submitted manuscripts sometimes focus on this questionable aspect. The literature on "remediations using Fe^0" is an illustration of the fact that bias can be introduced in the scientific literature and maintained for decades. In particular, the mechanism discussed here started in 1994 [16], but Khudenko [77] has been completely ignored since then; yet, this should be the starting point. The concept that Fe^0 is an environmental-reducing agent has never been established, as recently demonstrated by Ebelle et al. [75], but is still prevailing in both the old and recent literature [84–87].

By using a pyrite mineral in April 2019 (pristine FeS_2) and the same six months later (aged FeS_2), this work has critically evaluated the state-of-the-art knowledge on the mechanism of contaminant removal in Fe^0/H_2O systems in a unique way. An array of experimental conditions could be created that would have been difficult to conciliate if they were not from the same set of experiments. In particular, the fact that decreased pH values (or increased iron concentrations) (Figure 1) should never be randomly interchanged with increased contaminant removal is elegantly demonstrated (Figure 5). Figure 5 represents the results of 102 experimental points obtained herein and by Cui [88] in investigating the $Fe^0/FeS_2/H_2O$ system using MB, MO, and RR120. Figure 5a shows clearly that, regardless of the used dye, the dissolved iron level decreased with the increasing pH values. In all the systems, the initial pH value was 6.8 ± 0.2. There is thus no doubt that the FeS_2 addition decreases the pH value and increases the iron concentrations. The extent of the dye discoloration in each system depends on several operation parameters that determine the minimum value (e.g., <4.5 for pristine FeS_2) and the final pH value. Sections 3.1–3.3 have presented the results for individual systems. Figure 5b summarizes the pH dependence of the E values. It is seen that the values are scattered without any trend, unlike for the iron level (Figure 5a).

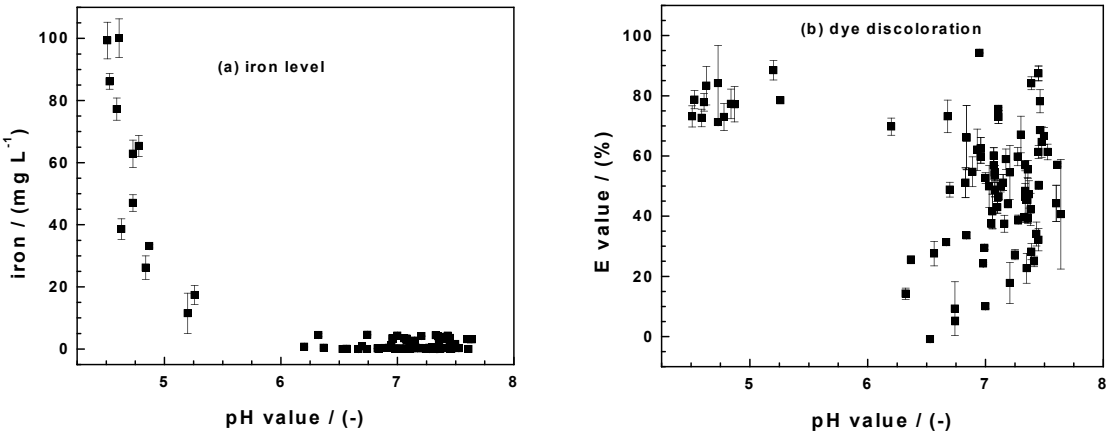

Figure 5. Summary of the pH dependence of (**a**) the iron concentration and (**b**) the extent of dye discoloration (E value) obtained herein and by Cui [88] while investigating the $Fe^0/FeS_2/H_2O$ systems for the discoloration of methylene blue (MB), methyl orange (MO), and reactive red 120. 102 triplicate experiments were performed. The initial pH was 6.8 ± 0.2; data are not sorted.

It is hoped that, in establishing that contaminant removals in Fe^0/H_2O systems are due to flocculation (adsorption and coprecipitation) (Figure 6) [89], the results presented herein will redirect the research for the design of the next generation of Fe^0-based remediation systems, accounting for the ion-selective nature of the systems [14,84,89–92]. The view that Fe^0 is a reducing agent [15,93,94]

should be immediately abandoned [85]. This view has mediated or supported wrong wordings like zero-valent iron for metallic [14] or reductates for species reducible by Fe^0 according to the relative electrode potentials [94]. In 2013, the notion of electron efficiency was introduced [86,95,96] and has been progressively used by several research groups [86]. The electron efficiency concept strives to reduce Fe^0 wastage by accounting for the redistribution of electrons from Fe^0 to (i) target (reducible) contaminants (e.g., MO), (ii) dissolved oxygen (O_2), and (iii) reducible co-contaminants like nitrate (NO_3^-) [86]. The present work has documented intensive Fe^0 oxidation without MO reduction. Accordingly, contaminant reductive transformation is the consequence and not the cause or one of the causes of Fe^0 oxidative dissolution.

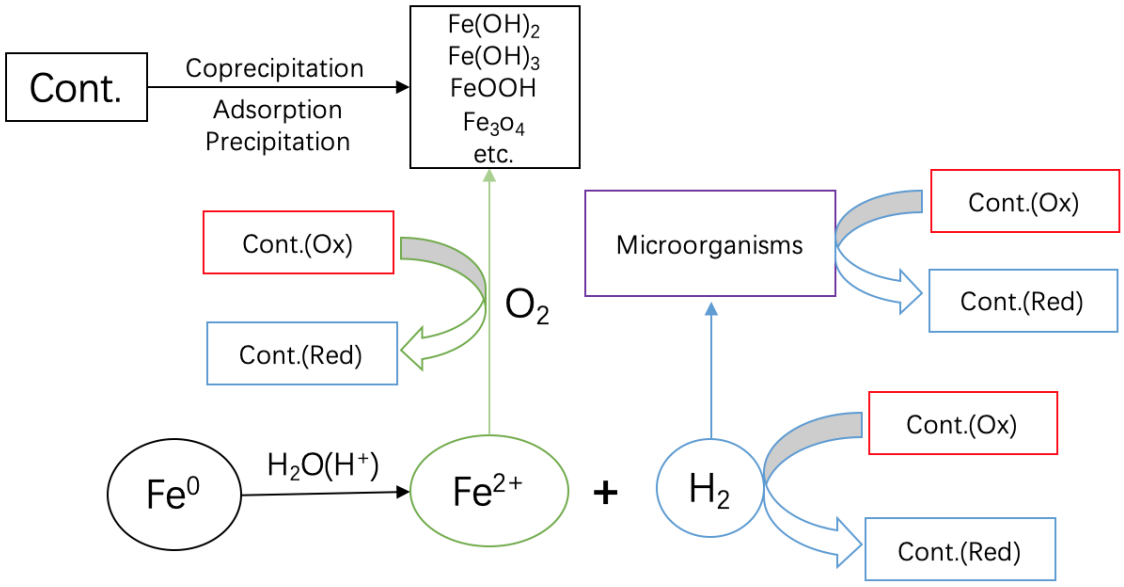

Figure 6. Scheme showing the pathways of contaminant removal and transformations in Fe^0/H_2O systems. Only water has access to the metal surface. Fe^{2+} and H_2 are stand-alone reducing agents. O_2 is reduced by Fe^{2+}. H_2 can be used by microorganisms to induce redox transformations of dissolved species. Upon the oxidation of Fe^{2+}, various solid iron hydroxides/oxides precipitate and act as contaminant scavengers.

Finally, the very recent results of Seng et al. [49] demonstrate on a purely thermodynamic perspective that Fe^0 should be used to stop FeS_2 oxidation. In other words, upon immersion, the FeS_2 surface is progressively coated by FeCPs from anodic Fe^0 oxidation. Since the opposite has been favored and largely documented in the Fe^0 remediation literature [15,29,69,76], it is time for more detailed investigations. The present work provides a kinetic-based answer, suggesting that more attention should be paid to the relative dissolution rate of both Fe^0 and FeS_2. In particular, the suitability of MB as an operational tracer for the reactivity of the dynamic Fe^0/H_2O system is corroborated. It is very important to state that the MB method is complementing knowledge from the conventional approach while simultaneously providing further insights into the dynamic aspects. Conventionally, dynamic interactions between reactive materials (e.g., Fe^0 and FeS_2.) and dissolved species (e.g., contaminants and O_2) are investigated by employing a suite of solution chemistry and solid-phase characterization approaches [49,86,97–100]. The achieved results are then used to develop a time series correlation analysis justifying the contaminant removal or transformation in the Fe^0/H_2O system [99].

4. Concluding Remarks

The concept that contaminant removal in Fe^0/H_2O systems is caused by the precipitation of solid iron corrosion products (FeCPs) is consistent with many experimental observations. A FeS_2 addition

induces a shift of the pH to lower values, but this process is only associated with contaminant removal when quantitative precipitation occurs. Contaminants are removed by adsorption onto FeCPs or occlusion in precipitating FeCPs (coprecipitation). Further, the relative importance of adsorption and coprecipitation can only be speculatively discussed due to the dynamic nature of the system and the difficulty to perform Fe mass balance. The expected ion-selective nature of the Fe^0/H_2O system is demonstrated by the differential discoloration of MB and MO. The comparatively higher removal of RR120 is justified by steric effects and its lower solubility. Finally, the differential reactivity of pristine and aged FeS_2 shows that both Fe^0 and reactive additives have to be characterized for their initial intrinsic reactivity and the long-term kinetics of oxidative dissolution. This observation calls for more systematic investigations for the design of the next generation of Fe^0-based remediation systems.

Author Contributions: Funding acquisition, R.H.; Investigation, M.X. and X.C.; Methodology, C.N. and W.G.; Supervision, C.N. and R.H.; And writing—review and editing, W.G. All authors have read and agreed to the published version of the manuscript.

Funding: This work was supported by the Ministry of Science and Technology of China through the Program "Research on Mechanism of Groundwater Exploitation and Seawater Intrusion in Coastal Areas" (Project Code 20165037412) and Postgraduate Research & Practice Innovation Program of Jiangsu Province (Project Code: SJKY19_0519, 2019B60214)

Acknowledgments: The used pyrite mineral (FeS_2) was kindly donated by Yimin Li from the College of Chemistry418 and Chemical Engineering, Shaoxing University, China. Huichen Yang (University of Göttingen) is thanked for the technical support. The manuscript was improved by the insightful comments of anonymous reviewers from Water. We acknowledge support by the German Research Foundation and the Open Access Publication Funds of Göttingen University.

Conflicts of Interest: The authors declare no conflict of interest.

References

1. Bischof, G. *The Purification of Water: Embracing the Action of Spongy Iron on Impure Water*; Bell and Bain: Glasgow, Scotland, 1873; p. 19.
2. Devonshire, E. The purification of water by means of metallic iron. *J. Frankl. Inst.* **1890**, *129*, 449–461. [CrossRef]
3. Lauderdale, R.A.; Emmons, A.H. A method for decontaminating small volumes of radioactive water. *J. Am. Water Works Ass.* **1951**, *43*, 327–331. [CrossRef]
4. Guan, X.; Sun, Y.; Qin, H.; Li, J.; Lo, I.M.C.; He, D.; Dong, H. The limitations of applying zero-valent iron technology in contaminants sequestration and the corresponding countermeasures: The development in zero-valent iron technology in the last two decades (1994–2014). *Water Res.* **2015**, *75*, 224–248. [CrossRef] [PubMed]
5. Mwakabona, H.T.; Ndé-Tchoupé, A.I.; Njau, K.N.; Noubactep, C.; Wydra, K.D. Metallic iron for safe drinking water provision: Considering a lost knowledge. *Water Res.* **2017**, *117*, 127–142. [CrossRef]
6. Noubactep, C. Metallic iron for environmental remediation: Prospects and limitations. In *A Handbook of Environmental Toxicology: Human Disorders and Ecotoxicology*; Chapter 36; D'Mello, J.P.F., Ed.; CAB International: Wallingford, UK, 2019; pp. 531–544.
7. O'Hannesin, S.F.; Gillham, R.W. Long-term performance of an In Situ "iron wall" for remediation of VOCs. *Ground Water* **1998**, *36*, 164–170. [CrossRef]
8. Richardson, J.P.; Nicklow, J.W. In Situ permeable reactive barriers for groundwater contamination. *Soil Sediment Contam.* **2002**, *11*, 241–268. [CrossRef]
9. Henderson, A.D.; Demond, A.H. Long-term performance of zero-valent iron permeable reactive barriers: A critical review. *Environ. Eng. Sci.* **2007**, *24*, 401–423. [CrossRef]
10. Gheju, M. Hexavalent chromium reduction with zero-valent iron (ZVI) in aquatic systems. *Water Air Soil Pollut.* **2011**, *222*, 103–148. [CrossRef]
11. Obiri-Nyarko, F.; Grajales-Mesa, S.J.; Malina, G. An overview of permeable reactive barriers for in situ sustainable groundwater remediation. *Chemosphere* **2014**, *111*, 243–259. [CrossRef] [PubMed]
12. Ghauch, A. Iron-based metallic systems: An excellent choice for sustainable water treatment. *Freib. Online Geosci.* **2015**, *32*, 1–80.

13. Antia, D.D.J. ZVI (Fe^0) Desalination: Stability of product water. *Resources* **2016**, *5*, 15. [CrossRef]
14. Xiao, M.; Hu, R.; Cui, X.; Gwenzi, W.; Noubactep, C. Understanding the operating mode of Fe^0/Fe-sulfide/H_2O systems for water treatment. *Processes* **2020**, *8*, 409. [CrossRef]
15. Chen, K.; Han, L.; Li, J.; Lü, Y.; Yao, C.; Dong, H.; Wang, L.; Li, Y. Pyrite enhanced the reactivity of zero valent iron for reductive removal of dyes. *J. Chem. Technol. Biotechnol.* **2020**. [CrossRef]
16. Matheson, L.J.; Tratnyek, P.G. Reductive dehalogenation of chlorinated methanes by iron metal. *Environ. Sci. Technol.* **1994**, *28*, 2045–2053. [CrossRef]
17. Jiao, Y.; Qiu, C.; Huang, L.; Wu, K.; Ma, H.; Chen, S.; Ma, L.; Wu, L. Reductive dechlorination of carbon tetrachloride by zero-valent iron and related iron corrosion. *Appl. Catal. B Environ.* **2009**, *91*, 434–440. [CrossRef]
18. Noubactep, C. Processes of contaminant removal in "Fe^0–H_2O" systems revisited. The importance of co-precipitation. *Open Environ. Sci.* **2007**, *1*, 9–13. [CrossRef]
19. Noubactep, C. A critical review on the mechanism of contaminant removal in Fe^0–H_2O systems. *Environ. Technol.* **2008**, *29*, 909–920. [CrossRef]
20. Ghauch, A.; Abou, A.H.; Bdeir, S. Aqueous removal of diclofenac by plated elemental iron: Bimetallic systems. *J. Hazard. Mater.* **2010**, *182*, 64–74. [CrossRef]
21. Ghauch, A.; Abou Assi, H.; Baydoun, H.; Tuqan, A.M.; Bejjani, A. Fe0-based trimetallic systems for the removal of aqueous diclofenac: Mechanism and kinetics. *Chem. Eng. J.* **2011**, *172*, 1033–1044. [CrossRef]
22. Gheju, M.; Balcu, I. Removal of chromium from Cr(VI) polluted wastewaters by reduction with scrap iron and subsequent precipitation of resulted cations. *J. Hazard. Mater.* **2011**, *196*, 131–138. [CrossRef] [PubMed]
23. Bartzas, G.; Komnitsas, K. Solid phase studies and geochemical modelling of low-cost permeable reactive barriers. *J. Hazard. Mater.* **2010**, *183*, 301–308. [CrossRef] [PubMed]
24. Li, L.; Benson, C.H. Evaluation of five strategies to limit the impact of fouling in permeable reactive barriers. *J. Hazard. Mater.* **2010**, *181*, 170–180. [CrossRef]
25. Noubactep, C. Metallic iron for environmental remediation: A review of reviews. *Water Res.* **2015**, *85*, 114–123. [CrossRef]
26. Noubactep, C.; Schöner, A.; Sauter, M. Significance of oxide-film in discussing the mechanism of contaminant removal by elemental iron materials. In *Photo-Electrochemistry and Photo-Biology for the Sustainability*; Union Press: Osaka, Japan, 2012; pp. 97–122.
27. Huang, Y.H.; Peddi, P.K.; Zeng, H.; Tang, C.-L.; Teng, X. Pilot-scale demonstration of the hybrid zero-valent iron process for treating flue-gas-desulfurization wastewater: Part, I. *Water Sci. Technol.* **2013**, *67*, 16–23. [CrossRef] [PubMed]
28. Huang, Y.H.; Tang, C.; Zeng, H. Removing molybdate from water using a hybridized zero-valent iron/magnetite/Fe(II) treatment system. *Chem. Eng. J.* **2012**, *200–202*, 257–263. [CrossRef]
29. Lü, Y.; Li, J.F.; Li, Y.M.; Liang, L.P.; Dong, H.P.; Chen, K.; Yao, C.; Li, Z.; Li, J.; Guan, X. The roles of pyrite for enhancing reductive removal of nitrobenzene by zero-valent iron. *Appl. Catal. B Environ.* **2019**, *242*, 9–18. [CrossRef]
30. Btatkeu-K, B.D.; Olvera-Vargas, H.; Tchatchueng, J.B.; Noubactep, C.; Caré, S. Characterizing the impact of MnO_2 on the efficiency of Fe^0-based filtration systems. *Chem. Eng. J.* **2014**, *250*, 416–422. [CrossRef]
31. Gheju, M.; Balcu, I. Sustaining the efficiency of the Fe(0)/H_2O system for Cr(VI) removal by MnO_2 amendment. *Chemosphere* **2019**, *214*, 389–398. [CrossRef]
32. Westerhoff, P.; James, J. Nitrate removal in zero-valent iron packed columns. *Water Res.* **2003**, *37*, 1818–1830. [CrossRef]
33. Song, D.-I.; Kim, Y.H.; Shin, W.S. A simple mathematical analysis on the effect of sand in Cr(VI) reduction using zero valent iron. *Korean J. Chem. Eng.* **2005**, *22*, 67–69. [CrossRef]
34. Bi, E.; Devlin, J.F.; Huang, B. Effects of mixing granular iron with sand on the kinetics of trichloroethylene reduction. *Ground Water Monit. Remed.* **2009**, *29*, 56–62. [CrossRef]
35. Hu, R.; Yang, H.; Tao, R.; Cui, X.; Xiao, M.; Konadu-Amoah, B.; Cao, V.; Lufingo, M.; Soppa-Sangue, N.P.; Ndé-Tchoupé, A.I.; et al. Metallic iron for environmental remediation: Starting an overdue progress in knowledge. *Water* **2020**, *12*, 641. [CrossRef]
36. Hu, R.; Gwenzi, W.; Sipowo-Tala, V.R.; Noubactep, C. Water treatment using metallic iron: A tutorial review. *Processes* **2019**, *7*, 622. [CrossRef]

37. Miyajima, K.; Noubactep, C. Effects of mixing granular iron with sand on the efficiency of methylene blue discoloration. *Chem. Eng. J.* **2012**, *200–202*, 433–438. [CrossRef]
38. Kim, H.; Yang, H.; Kim, J. Standardization of the reducing power of zerovalent iron using iodine. *Environ. Lett.* **2014**, *49*, 514–523.
39. Li, S.; Ding, Y.; Wang, W.; Lei, H. A facile method for determining the Fe(0) content and reactivity of zero valent iron. *Anal. Methods* **2016**, *8*, 1239–1248. [CrossRef]
40. Miyajima, K. Optimizing the design of metallic iron filters for water treatment. *Freib. Online Geosci.* **2012**, *32*, 1–60.
41. Btatkeu-K, B.D.; Tchatchueng, J.B.; Noubactep, C.; Caré, S. Designing metallic iron based water filters: Light from methylene blue discoloration. *J. Environ. Manag.* **2016**, *166*, 567–573. [CrossRef]
42. Mitchell, G.; Poole, P.; Segrove, H.D. Adsorption of methylene blue by high-silica sands. *Nature* **1955**, *176*, 1025–1026. [CrossRef]
43. Noubactep, C.; Meinrath, G.; Dietrich, P.; Merkel, B. Mitigating uranium in groundwater: Prospects and limitations. *Environ. Sci. Technol.* **2003**, *37*, 4304–4308. [CrossRef] [PubMed]
44. Noubactep, C.; Meinrath, G.; Merkel, J.B. Investigating the mechanism of uranium removal by zerovalent iron materials. *Environ. Chem.* **2005**, *2*, 235–242. [CrossRef]
45. Gatcha-Bandjun, N.; Noubactep, C.; Loura, B.B. Mitigation of contamination in effluents by metallic iron: The role of iron corrosion products. *Environ. Technol. Innov.* **2017**, *8*, 71–83. [CrossRef]
46. Groysman, A. *Corrosion for Everybody*; Springer: Dordrecht, The Netherlands, 2010; p. 368.
47. Chopard, A.; Benzaazoua, M.; Bouzahzah, H.; Plante, B.; Marion, P. A contribution to improve the calculation of the acid generating potential of mining wastes. *Chemosphere* **2017**, *175*, 97–107. [CrossRef] [PubMed]
48. Chopard, A.; Marion, P.; Mermillod-Blondin, R.; Plante, B.; Benzaazoua, M. Environmental impact of mine exploitation: An early predictive methodology based on ore mineralogy and contaminant speciation. *Minerals* **2019**, *9*, 397. [CrossRef]
49. Seng, S.; Tabelin, C.B.; Kojima, M.; Hiroyoshi, N.; Ito, M. Galvanic microencapsulation (GME) using zero-valent aluminum and zero-valent iron to suppress pyrite oxidation. *Mater. Trans.* **2019**, *60*, 277–286. [CrossRef]
50. Tabelin, C.B.; Park, I.; Li, X.; Seng, S.; Villacorte-Tabelin, M.; Igarashi, T.; Ito, M.; Hiroyoshi, N. Development of advanced pyrite passivation strategies towards sustainable management of acid mine drainage. *IOP Conf. Ser. Earth Environ. Sci.* **2019**, *351*. [CrossRef]
51. Rodríguez, A.; García, J.; Ovejero, G.; Mestanza, M. Adsorption of anionic and cationic dyes on activated carbon from aqueous solutions: Equilibrium and kinetics. *J. Hazard. Mater.* **2009**, *172*, 1311–1320. [CrossRef]
52. Attia, A.A.; Girgis, B.S.; Fathy, N.A. Removal of methylene blue by carbons derived from peach stones by H_3PO_4 activation: Batch and column studies. *Dyes Pigment.* **2008**, *76*, 282–289. [CrossRef]
53. Frost, R.L.; Xi, Y.; He, H. Synthesis, characterization of palygorskite supported zero-valent iron and its application for methylene blue adsorption. *J. Colloid Interface Sci.* **2010**, *341*, 153–161. [CrossRef]
54. Huang, J.H.; Huang, K.L.; Liu, S.Q.; Wang, A.T.; Yan, C. Adsorption of Rhodamine B and methyl orange on a hypercrosslinked polymeric adsorbent in aqueous solution. *Colloids Surf. A Physicochem. Eng. Asp.* **2008**, *330*, 55–61. [CrossRef]
55. Phukan, M.; Noubactep, C.; Licha, T. Characterizing the ion-selective nature of Fe^0-based filters using azo dyes. *Chem. Eng. J.* **2015**, *259*, 481–491. [CrossRef]
56. Hu, R.; Cui, X.; Xiao, M.; Qiu, P.; Lufingo, M.; Gwenzi, W.; Noubactep, C. Characterizing the suitability of granular Fe^0 for the water treatment industry. *Processes* **2019**, *7*, 652. [CrossRef]
57. Lufingo, M.; Ndé-Tchoupé, A.I.; Hu, R.; Njau, K.N.; Noubactep, C. A novel and facile method to characterize the suitability of metallic iron for water treatment. *Water* **2019**, *11*, 2465. [CrossRef]
58. Miyajima, K.; Noubactep, C. Characterizing the impact of sand addition on the efficiency of granular iron for water treatment. *Chem. Eng. J.* **2015**, *262*, 891–896. [CrossRef]
59. Btatkeu-K, B.D.; Olvera-Vargas, H.; Tchatchueng, J.B.; Noubactep, C.; Caré, S. Determining the optimum Fe^0 ratio for sustainable granular Fe^0/sand water filters. *Chem. Eng. J.* **2014**, *247*, 265–274. [CrossRef]
60. Varlikli, C.; Bekiari, V.; Kus, M.; Boduroglu, N.; Oner, I.; Lianos, P.; Lyberatos, G.; Icli, S. Adsorption of dyes on Sahara desert sand. *J. Hazard. Mater.* **2009**, *170*, 27–34. [CrossRef]
61. Miyajima, K.; Noubactep, C. Impact of Fe^0 amendment on methylene blue discoloration by sand columns. *Chem. Eng. J.* **2013**, *217*, 310–319. [CrossRef]

62. Lipczynska-Kochany, E.; Harms, S.; Milburn, R.; Sprah, G.; Nadarajah, N. Degradation of carbon tetrachloride in the presence of iron and sulphur containing compounds. *Chemosphere* **1994**, *29*, 1477–1489. [CrossRef]
63. Shiba, M.; Uddin, M.A.; Kato, Y.; Ono, T. Degradation of chlorinated organic compounds by mixed particles of iron/iron sulfide or iron/iron disulfide. *Mater. Trans.* **2014**, *55*, 708–712. [CrossRef]
64. Kantar, C.; Ari, C.; Keskin, S.; Dogaroglu, Z.G.; Karadeniz, A.; Alten, A. Cr(VI) removal from aqueous systems using pyrite as the reducing agent: Batch, spectroscopic and column experiments. *J. Contam. Hydrol.* **2015**, *174*, 28–38. [CrossRef]
65. Kantar, C.; Bulbul, M.S. Effect of pH-buffering on Cr(VI) reduction with pyrite in the presence of various organic acids: Continuous-flow experiments. *Chem. Eng. J.* **2016**, *287*, 173–180. [CrossRef]
66. Saywell, L.G.; Cunningham, B.B. Determination of iron: Colorimetric o-phenanthroline method. *Ind. Eng. Chem. Anal. Ed.* **1937**, *9*, 67–69. [CrossRef]
67. Du, M.; Zhang, Y.; Hussain, I.; Du, X.; Huang, S.; Wen, W. Effect of pyrite on enhancement of zero-valent iron corrosion for arsenic removal in water: A mechanistic study. *Chemosphere* **2019**, *233*, 744–753. [CrossRef] [PubMed]
68. Noubactep, C.; Caré, S.; Crane, R.A. Nanoscale metallic iron for environmental remediation: Prospects and limitations. *Water Air Soil Pollut.* **2012**, *223*, 1363–1382. [CrossRef]
69. Lavine, B.K.; Auslander, G.; Ritter, J. Polarographic studies of zero valent iron as a reductant for remediation of nitroaromatics in the environment. *Microchem. J.* **2001**, *70*, 69–83. [CrossRef]
70. Phukan, M.; Noubactep, C.; Licha, T. Characterizing the ion-selective nature of Fe^0-based filters using three azo dyes in batch systems. *J. Environ. Chem. Eng.* **2016**, *4*, 65–72. [CrossRef]
71. Phukan, M. Characterizing the Fe^0/sand system by the extent of dye discoloration. *Freiberg Online Geosci.* **2015**, *40*, 1–70.
72. Bradley, I.; Straub, A.; Maraccini, P.; Markazi, S.; Nguyen, T.H. Iron oxide amended biosand filters for virus removal. *Water Res.* **2011**, *45*, 4501–4510. [CrossRef]
73. Noubactep, C.; Schöner, A.; Woafo, P. Metallic iron filters for universal access to safe drinking water. *Clean Soil Air Water* **2009**, *37*, 930–937. [CrossRef]
74. Nanseu-Njiki, C.P.; Gwenzi, W.; Pengou, M.; Rahman, M.A.; Noubactep, C. Fe^0/H_2O filtration systems for decentralized safe drinking water: Where to from here? *Water* **2019**, *11*, 429. [CrossRef]
75. Ebelle, T.C.; Makota, S.; Tepong-Tsindé, R.; Nassi, A.; Noubactep, C. Metallic iron and the dialogue of the deaf. *Fresenius Environ. Bull.* **2019**, *28*, 8331–8340.
76. Lü, Y.; Li, Z.F.; Li, J.F.; Chen, K.; Dong, H.P.; Shou, J.X.; Li, Y. Synergetic effect of pyrite on Cr(VI) removal by zero valent iron in column experiments: An investigation of mechanisms. *Chem. Eng. J.* **2018**, *349*, 522–529. [CrossRef]
77. Khudenko, B.M. Feasibility evaluation of a novel method for destruction of organics. *Water Sci. Technol.* **1991**, *23*, 1873–1881. [CrossRef]
78. Noubactep, C.; Meinrath, G.; Volke, P.; Peter, H.-J.; Dietrich, P.; Merkel, B. *Understanding the Mechanism of the Uranium Mitigation by Zero Valent Iron in Effluents*; Wiss. Mitt. Institut für Geologie der TU Bergakademie Freiberg: Freiberg, Germany, 2001; pp. 37–44.
79. Noubactep, C.; Meinrath, G.; Volke, P.; Dietrich, P.; Merkel, B.J. Mechanisms of uranium fixation by zero valent iron: The importance of co-precipitation. In *Uranium in the Aquatic Environment*; Springer: Berlin/Heidelberg, Germany, 2002; pp. 577–586.
80. Howe, K.J.; Hand, D.W.; Crittenden, J.C.; Trussell, R.R.; Tchobanoglous, G. *Principles of Water Treatment*; John Wiley & Sons, Inc.: Hoboken, NJ, USA, 2012; p. 647.
81. Crawford, R.J.; Harding, I.H.; Mainwaring, D.E. Adsorption and coprecipitation of single heavy metal ions onto the hydrated oxides of iron and chromium. *Langmuir* **1993**, *9*, 3050–3056. [CrossRef]
82. Crawford, R.J.; Harding, I.H.; Mainwaring, D.E. Adsorption and coprecipitation of multiple heavy metal ions onto the hydrated oxides of iron and chromium. *Langmuir* **1993**, *9*, 3057–3062. [CrossRef]
83. Noubactep, C.; Schöner, A.; Meinrath, G. Mechanism of uranium removal from the aqueous solution by elemental iron. *J. Hazard. Mater.* **2006**, *132*, 202–212. [CrossRef] [PubMed]
84. Antia, D.D.J. Water treatment and desalination using the eco-materials n-Fe^0 (ZVI), n-Fe_3O_4, n-$Fe_xO_yH_z$[mH_2O], and n-Fex[Cation]nOyHz[Anion]m [rH_2O]. In *Handbook of Nanomaterials and Nanocomposites for Energy and Environmental Applications*; Springer Nature: Cham, Switzerland, 2020.

85. Cao, V.; Yang, H.; Ndé-Tchoupé, A.I.; Hu, R.; Gwenzi, W.; Noubactep, C. Tracing the Scientific History of Fe^0-Based Environmental Remediation Prior to the Advent of Permeable Reactive Barriers. *Processes* **2020**, *8*, 977. [CrossRef]
86. He, F.; Gong, L.; Fan, D.; Tratnyek, P.G.; Lowry, G.V. Quantifying the efficiency and selectivity of organohalide dechlorination by zerovalent iron. *Environ. Sci. Process. Impacts* **2020**, *22*, 528. [CrossRef]
87. Yang, H.; Hu, R.; Ndé-Tchoupé, A.I.; Gwenzi, W.; Ruppert, H.; Noubactep, C. Designing the next generation of Fe^0-based filters for decentralized safe drinking water treatment: A conceptual framework. *Processes* **2020**, *8*, 745. [CrossRef]
88. Cui, X. Study on the Material Selection of Zero Valent Iron Permeable Reactive Barrier and the Effect of Pyrite on Its Treatment Efficiency. Master's Thesis, Hohai University, Nanjing, China, 2020. (In Chinese).
89. Bojic, A.L.; Bojic, D.; Andjelkovic, T. Removal of Cu^{2+} and Zn^{2+} from model wastewaters by spontaneous reduction–coagulation process in flow conditions. *J. Hazard. Mater.* **2009**, *168*, 813–819. [CrossRef]
90. Sato, N. Surface oxides affecting metallic corrosion. *Corros. Rev.* **2001**, *19*, 253–272. [CrossRef]
91. Ullah, S.; Guo, X.; Luo, X.; Zhang, X.; Li, Y.; Liang, Z. The coupling of sand with ZVI/oxidants achieved proportional and highly efficient removal of arsenic. Front. *Environ. Sci. Eng.* **2020**, *14*, 94.
92. Heimann, S.; Ndé-Tchoupé, A.I.; Hu, R.; Licha, T.; Noubactep, C. Investigating the suitability of Fe^0 packed-beds for water defluoridation. *Chemosphere* **2018**, *209*, 578–587. [CrossRef]
93. Roberts, A.L.; Totten, L.A.; Arnold, W.A.; Burris, D.R.; Campbell, T.J. Reductive elimination of chlorinated ethylenes by zero-valent metals. *Environ. Sci. Technol.* **1996**, *30*, 2654–2659. [CrossRef]
94. Miehr, R.; Tratnyek, P.G.; Bandstra, Z.J.; Scherer, M.M.; Alowitz, J.M.; Bylaska, J.E. Diversity of contaminant reduction reactions by zerovalent iron: Role of the reductate. *Environ. Sci. Technol.* **2004**, *38*, 139–147. [CrossRef]
95. Liu, H.; Wang, Q.; Wang, C.; Li, X.-z. Electron efficiency of zero-valent iron for groundwater remediation and wastewater treatment. *Chem. Eng. J.* **2013**, *215–216*, 90–95. [CrossRef]
96. Wu, C.-Q.; Fu, D.-T.; Chen, X. Nitrobenzene degradation by micro-sized iron and electron efficiency evaluation. *Chem. Pap.* **2014**, *68*, 1350–1357. [CrossRef]
97. Gillham, R.W. Development of the granular iron permeable reactive barrier technology (good science or good fortune). In *Advances in Environmental Geotechnics, Proceedings of the International Symposium on Geoenvironmental Engineering in Hangzhou, China, 8–10 September 2007*; Chen, Y., Tang, X., Zhan, L., Eds.; Springer: Berlin, Germany, 2008; pp. 5–15.
98. Duan, R.; Dong, Y.; Zhang, Q. Characteristics of aggregate size distribution of nanoscale zero-valent iron in aqueous suspensions and its effect on transport process in porous media. *Water* **2018**, *10*, 670. [CrossRef]
99. Shao, Q.; Xu, C.; Wang, Y.; Huang, S.; Zhang, B.; Huang, L.; Fan, D.; Tratnyek, P.G. Dynamic interactions between sulfidated zerovalent iron and dissolved oxygen: Mechanistic insights for enhanced chromate removal. *Water Res.* **2018**, *135*, 322–330. [CrossRef] [PubMed]
100. Mondino, F.; Piscitello, A.; Bianco, C.; Gallo, A.; de Folly D'Auris, A.; Tosco, T.; Tagliabue, M.; Sethi, R. Injection of zerovalent iron gels for aquifer nanoremediation: Lab experiments and modeling. *Water* **2020**, *12*, 826. [CrossRef]

© 2020 by the authors. Licensee MDPI, Basel, Switzerland. This article is an open access article distributed under the terms and conditions of the Creative Commons Attribution (CC BY) license (http://creativecommons.org/licenses/by/4.0/).